INFLUENCE OF FFF PROCESS PARAMETERS ON THE MECHANICAL PROPERTIES OF SINTERED 17-4PH STAINLESS STEEL

GYORGY LEDNICZKY[1], ADRIAN BOGNAR[1], KRISZTIAN KUN[1*], LASZLO ZSIDAI[2], ZOLTAN WELTSCH[3]

[1]John von Neumann University, Kecskemet, Hungary
[2]Hungarian University of Agriculture and Life Sciences, Godollo, Hungary
[3]Department of Road and Rail Vehicles, Zalaegerszeg Innovation Park, Szechenyi Istvan University, Gyor, Hungary

DOI: 10.17973/MMSJ.2025_11_2025126

e-mail: kun.krisztian@nje.hu

ABSTRACT

This study examines how Fused Filament Fabrication (FFF) process parameters affect the mechanical properties of sintered 17-4PH stainless steel. Test specimens were printed from BASF Ultrafuse 17-4PH filament on an IDEX system and processed by industrial debinding and sintering. The effects of layer height, printing speed and infill angle were evaluated through tensile testing. The highest tensile strength of 802 MPa was achieved at 0.2 mm layer height, 25 mm/s printing speed and 45° infill orientation. Layer height showed the dominant influence on tensile strength, as later confirmed by ANOVA, while printing speed and infill angle had smaller or non-significant effects within the tested range. The results give a practical understanding of how printing parameters determine the mechanical behavior of 17-4PH parts and can support further optimization of metal FFF processes.

KEYWORDS

fused filament fabrication, metal extrusion, stainless steel, additive manufacturing

1 INTRODUCTION

In the field of additive manufacturing, metal printing has a shorter research history compared to polymer-based processes, partly because it is still not a widely accessible or established technology. Nevertheless, interest in metal additive manufacturing has grown rapidly, as it enables the production of complex geometries that are difficult or impossible to achieve with conventional machining or molding methods. Metal printing technologies can be grouped into two main categories: powder-based and extrusion-based processes. Powder-based methods include Selective Laser Sintering (SLS), Selective Laser Melting (SLM), Direct Metal Laser Sintering (DMLS) and Laser Metal Deposition (LMD), while extrusion-based techniques involve plunger-, screw- or filament-based systems such as Fused Filament Fabrication (FFF). In the scientific literature, powder-based technologies are considerably more studied than extrusion-based metal printing. (Alami et al., 2023).

Metal printing technologies have distinct advantages and limitations. Powder-based methods produce smooth, nearly isotropic parts with complex internal geometries in a single step but require fine powders, costly equipment and strict safety precautions. Extrusion-based technologies provide larger build volumes, faster deposition and easier handling without such constraints. These processes create green parts containing a polymer binder, which must be removed by debinding before sintering at a temperature just below the alloy's melting point. Sintering consolidates the metal particles and results in about 12–20 % linear shrinkage. (Henry et al., 2021; Kedziora et al., 2022; Nurhudan et al., 2021; Zhang & Roch, 2022)

The literature review of FFF-based metal printing reveals several studies dealing with the correlation between printing parameters and the mechanical properties of sintered parts. Singh et al. (2021) investigated the optimal parameter settings for 17-4PH stainless steel and achieved a green part density of 4.91 g/cm³, demonstrating the influence of process parameters on part quality. This work provides a useful reference for designing experimental setups and supports the understanding of how parameter selection affects the mechanical performance of FFF-produced metal components. (G. Singh et al., 2021a).
Zhang Y. and colleagues, using 17-4PH metal powder, compared the mechanical properties of their proprietary blend material to those of test specimens produced by metal injection molding, and they concluded that it is possible to approach a tensile strength of 1000 MPa (Zhang & Roch, 2022).
Galantucci et al. (2022) compared 17-4PH specimens produced by different manufacturers and reported tensile strength values of about 800–900 MPa, while emphasizing the detrimental effect of porosity on mechanical performance. They concluded that the achievable tensile strength is approximately 800-900 MPa; however, they drew attention to the negative effects of porosity (Galantucci et al., 2022).Fazzini et al. investigated how printing parameters such as raster orientation affect the mechanical properties of sintered 17-4PH stainless steel. They found that the raster angle had a dominant influence, with stiffness changing by nearly 20 % and elongation decreasing when layers were oriented across the loading direction. Although the study identified key geometric effects, it did not analyze the combined influence of multiple parameters or their statistical interactions (Fazzini et al., 2023).Atatreh et al. (2023) examined the effect of different infill designs on the tensile strength and efficiency of FFF-printed metal parts. Their results showed that a solid infill improved tensile strength by about 42 % compared to a triangular infill pattern, but increased material usage and build time. However, the study was limited to infill geometry and did not include other process parameters such as layer height or printing speed(Atatreh et al., 2023).Singh et al. (2021) focused on Ti-6Al-4V alloy fabricated by metal fused filament fabrication to identify factors affecting final density and strength. They demonstrated that optimized extrusion temperature and sintering parameters could achieve relative densities above 90 % and mechanical properties comparable to MIM components. The research, however, was restricted to a single material system and did not consider detailed mechanical characterization beyond density and hardness(P. Singh et al., 2021).

Although the available studies have provided valuable knowledge about individual process parameters, the combined influence of multiple factors on the mechanical behavior of sintered 17-4PH stainless steel remains insufficiently explored. The aim of this article is to contribute to this area by experimentally analyzing how layer height, printing speed and infill orientation affect the tensile strength of FFF-produced 17-4PH parts. The novelty of this work lies in the construction of a parameter interaction diagram that visualizes the relationships among the investigated process variables and their joint effect on mechanical performance. This approach enables a clearer understanding of the correlations between process settings and final properties, providing a practical basis for optimizing FFF parameters in metal additive manufacturing.

2 MATERIALS AND METHODS

The sample's form was chosen based on the specimen commonly used in MIM. As raw material BASF Ultrafuse 17-4PH filament was used and CraftBot IDEX XL printer with CraftWare. The filament consists of metal powder and so called Catamold binder system, which is patented by BASF to create ready-to-use feedstock for powder injection molding of metals and ceramics. The material of the metal powder is a martensitic, precipitation hardening stainless steel, which has a wide range of application from aerospace to medical sector. It is well known due to its corrosion resistance, high impact strength and fracture toughness. There are more studies focusing on the microstructure, the behaviour of precipitation mechanism(BASF, 2024; Xometry, 2024).

For readers unfamiliar with this topic, **Figure 1** presents a flow chart illustrating the metal extrusion–based printing process. Although the process is not circular, this representation makes each step easier to follow.

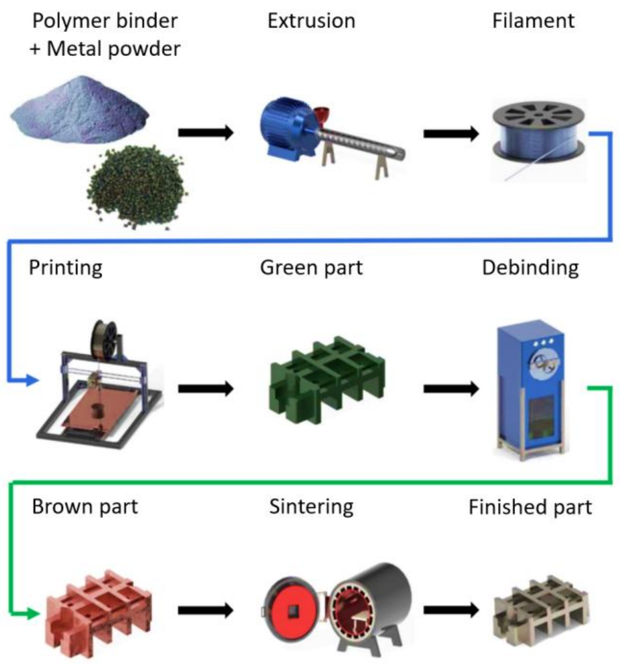

Figure 1. Metal extrusion based additive manufacturing process

The raw material is a homogeneous mixture of polymer binder and metal powder. The mixture's volumetric ratio is about 60% metal and 40% polymer, in mass ratio it is 90% metal and 10% polymer. The production and classification of fine metal powder is a complex industrial field. There are already some existing ISO standards regarding powder production and additive manufacturing, which indicates the unification to help both manufacturers and end-users as well.

After mixing the raw components, filaments are formed by extrusion. It may seem to be an easy step but taking into consideration just the tolerance of the filament's diameter, ±0.5 mm at 2.85 mm from BASF, then it's already not. Furthermore, the filament is needed to be spooled and later also extruded through the nozzle of a printer. Physical properties of the filaments, like flexibility and rigidity can change based on their manufacturer (Suwanpreecha & Manonukul, 2022).

After installing the BASF filament and slicing the CAD model, the green parts were printed with 100% infill. An experiment was planned, and the details will be explained in the following section. The parts' weight was measured by each and the distance of holes to determine later the shrinkage and weight loss.

The print speed basically affects the speed at which the print head moves, and therefore the printing time. However, it may also affect the degree of adhesion between the layers, so that even the tensile strength may vary. Although the manufacturer's recommendation allows higher values for printing speed, in our case filament jamming was detected by the printer. The print speed values were therefore chosen from a lower range. The layer height determines how thick the software should slice the CAD model into layers. The smaller the layer height, the more aesthetically pleasing and accurate the part, but the longer the printing time. In all cases, the fill orientation was parallel lines, and their angle was varied relative to the XY plane (BASF, 2024; Ozsoy et al., 2021; Pellegrini et al., 2023).

2.1 Catalytic binder reduction

For debinding and sintering Elnik Systems's service was used, which is accredited and appropriate to BASF's recommendation. The company is located in Germany, so the parts should be sent there after the proper number of vouchers are bought based on the weight of our green parts, and it took altogether a week to receive the parts back. The technology of debinding and sintering requires special equipment and chemical material, that's why there are few companies offering this service in Europe. Due to a request via email, Elnik Systems gave some details about sintering and debinding. The machines can be found on their website, but the details about the processing not. Different metal powders and binder systems require different way of sintering and debinding. Elnik Systems gives the opportunity to process 316L (1.4404) and 17-4PH (1.4542) materials. The mechanical properties of final parts are strongly influenced by the parameters of D&S process (Cho et al., 2023; Zhang & Roch, 2022b).

The workspace needs to be preheated to 120°C during the binder reduction process. After reaching the target temperature, heat retention for 45 minutes. After then begins the acid flow, which is done for an hour per one mm of wall thickness. The flow of acid is 3.4 ml/minute. Thereafter acid flow heat retention for 90 minutes at 120°C to clean the furnace and prepare to be opening. The used process shown in the **Figure 2.**

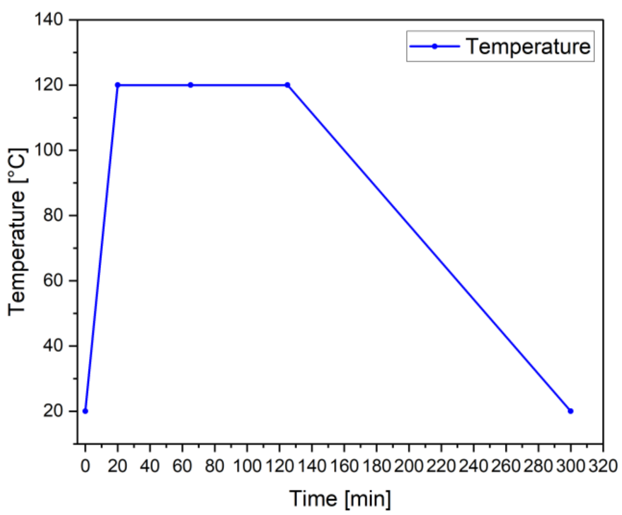

Figure 2. Diagram of debinding

For debinding Elnik Systems use their in-house developed machine, CD3045 furnace, which is adequate to debind BASF's patented Catamold binder system. The furnace is controlled by a PLC based PC and every process is recorded in Excel to improve the treatment (Elnik System, 2024).

2.2 Thermal binder removal and sintering

The sintering cycle begins with thermal debinding. Firstly, heat up to 450°C with 5°C/minutes heat ratio, then heat retention for 150 minutes. The next stage is 600°C, which is reached with 3°C/minutes heat ratio and heat retention for 60 minutes. The sintering stage of 1380°C is reached with 5°C/minutes heat ratio and heat retention for 180 minutes. Then let the furnace to cool down to room temperature **Figure 3.**

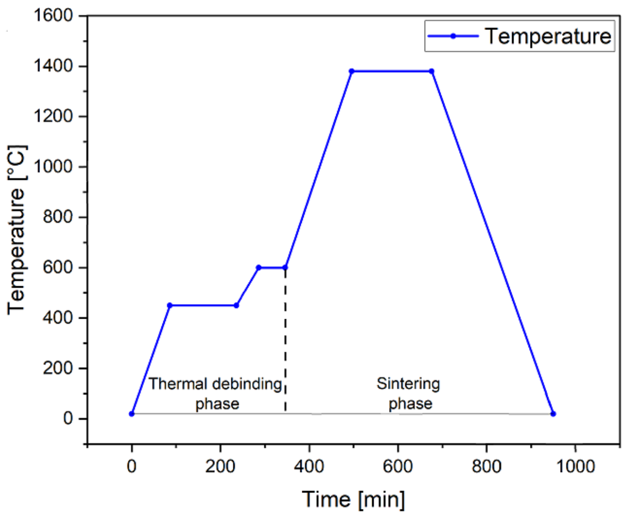

Figure 3. Diagram of sintering

The debinding and sintering furnaces are in-house developed equipment of Elnik Systems and MIM 3000 type is capable to carry out any metal's any kind of debinding at the same time before sintering, so the moving of parts can be avoided. This is provided by a gas tight refractory metal retort with a gas management system. Laminar gas flow guarantees the consistent properties of parts during every process.

After debinding and sintering final parts can be seen in **Figure 4.** compared with green parts.

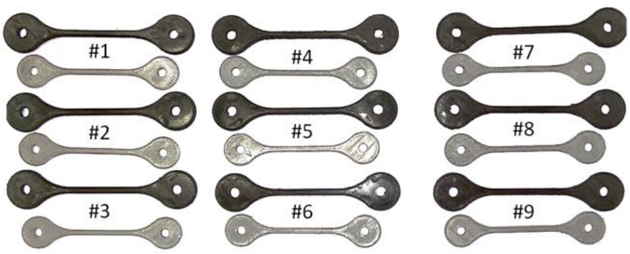

Figure 4. Green (printed) and sintered specimens

2.3 Experimental design

In order to achieve results for evaluation and analysis without trying every variation to examine the combined effect of several factors, thus spare much time and costs, it is a good practice to plan an experimental design. In engineering processes setups can be changed in much shorter time compared to an experiment in agriculture, which can even take years.

Common methods can be divided to three group:

- Factorial designs: simultaneous analysis of several factors,
- Response surface designs: in-depth analysis of correlations and modelling of characteristic curve fields,
- Quadratic designs: simultaneous investigation of more than two factors with more than two possible settings.

Factorial designs include one of the best-known experimental methodologies that allows a significant reduction in the number of experiments, by Genichi Taguchi. Two basic elements of Taguchi's approach are the loss function and the robust process model. With the loss function it is possible to describe deviations from the target value in financial units. The robust process model implies that processes should be made insensitive to disturbances and influencing factors. Taguchi considers the effect of controllable factors as a signal, and the effect of so-called noise factors as noise. The analysis based on the signal/noise ratio considers the mean of the repetitions and the standard deviation around the mean.

The mean squared deviation (MSD) is a function of the type of quality feature(Lenth, 2001):

- Nominal is best,
- Smaller is better,
- Larger is better (Minitab, 2024).

Based on preliminary printing and literature findings, three printing parameters were selected, which –according to our presumption- could influence the properties of the green and final parts and commonly used in plastic 3D printing.

The experiments involved three main process parameters: layer height, printing speed and infill angle. Based on the publications discussed in the Introduction, layer height values of 0.2 , 0.3 and 0.4 mm, printing speeds of 15, 25 and 35 mm/s, and infill angles of 0°, 45° and 90° were selected to study their influence on the final properties.(Galantucci et al., 2022; G. Singh et al., 2021a, 2021b; Zhang & Roch, 2022).

The parameters each could take up three value and so 9 different sets were set up. For each parameter combination, five specimens were produced in total, three of which were subjected to sintering, while two were retained in the green condition for comparison. The tensile test specimens were designed according to the MPIF Standard, which specifies a geometry optimized for Metal Injection Molding (MIM) due to its favorable flow characteristics. Using this geometry also enables direct comparison with results obtained from MIM-produced parts, making it a practical choice for the FFF process as well. The dimensions of the specimens are presented in the following **Figure 5.**

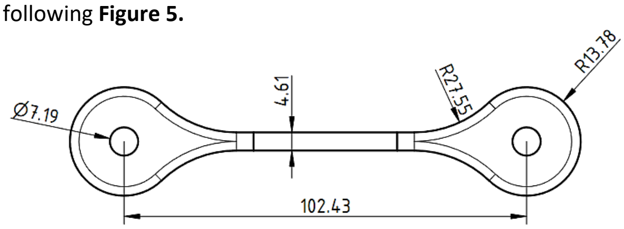

Figure 5. Dimensions of the MIM test specimen (MPIF Standard 50, 2000)

During the specimen fabrication, three different infill orientations were applied (0°, 45°, and 90°), as these can influence the mechanical properties in the tensile direction. The following **Figure 6** exported from the slicing software, illustrates the actual infill patterns used in the printed specimens.

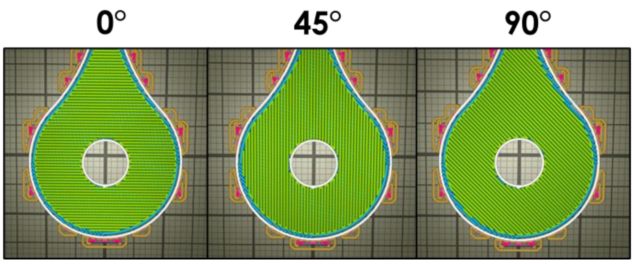

Figure 6 Infill orientation patterns (0°, 45°, and 90°) generated in the slicing software

The details of sets can be found in **Table 1.** Before selecting the values of printing speed and layer height, some trial printing had been done to see, if it's even possible to produce acceptable quality parts by looking. During preliminary trial prints, failed printing occurred when no adhesive (Magigoo) was applied, as recommended in the BASF datasheet to improve first-layer adhesion (BASF, 2024; Forward-am, 2024).

Experiment	Layer height [mm]	Printing speed [mm/s]	Infill angle [°]
1.	0.2	15	0
2.	0.2	25	45
3.	0.2	35	90
4.	0.3	15	45
5.	0.3	25	90
6.	0.3	35	0
7.	0.4	15	90
8.	0.4	25	0
9.	0.4	35	45

Table 1. Printing parameters for each set

2.4 Fracture surface observations and SEM analysis

Prior to the scanning electron microscopy, preliminary observations were performed on the fracture surfaces of the specimens that showed the highest tensile strength at each layer height. A Dino-Lite digital microscope was used to capture the surface morphology. For the detailed SEM analysis, a Zeiss Sigma 300 VP scanning electron microscope available at the university was employed. To improve visibility and surface evaluation, images were taken using both secondary electron (SE) and backscattered electron (BSD) detectors. The SEM micrographs presented in the paper were captured at 150× and 500× magnifications, revealing the characteristic fracture features and layer bonding quality of the sintered samples.

3 RESULTS

After receiving back the sintered parts, a tensile test was done without any cutting rework, like surface finishing. In order to determine linear shrinkage, hole distances were measured on green and final parts. The tensile test was carried out with Instron 5900R 4482 machine with 100 kN head. Depending on layer height, three sets were selected with the highest tensile strength results. The tensile test diagrams can be seen in **Figure 7,** where three different layer heights with a 45° infill orientation are presented to ensure relevant comparability, among which Exp. #2 achieved the highest tensile strength.

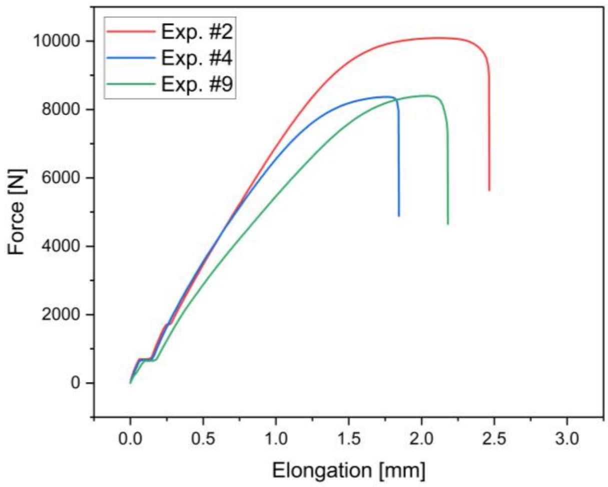

Figure 7. Comparison of Exp. 2., Exp. 4. and Exp. 9. produced by different parameters

The highest tensile stress was 797 MPa with #2, thus reaching 80% of BASF's value in the datasheet (BASF, 2024; Forward-am, 2024).
For better clarity and reproducibility, the tensile strength, strain at break and standard deviation values are summarized in **Table 2.** in numerical form.

Experiment	Stress [MPa] average	Strain [%] average	Standard deviation [MPa]
#1	754	2.3	4.6
#2	797	2.7	5.1
#3	682	1.9	7
#4	661	2.1	6.4
#5	577	1.6	124.7
#6	504	1.4	129.9
#7	609	1.8	20.2
#8	599	1.9	14.1
#9	655	2.0	11.0

Table 2. The results of the tensile tests of the specimens

From the values recorded during the mechanical tests, an analysis of the Taguchi experimental design was prepared. For the evaluation of the experiments, Taguchi experimental design was used to investigate the effect of the factors in Table 1. For each factor 3-3 variables were modified. The evaluations were carried out using Minitab software. The goal is to determine the highest possible tensile strength from the force values obtained from the tensile test, for which the 'larger is better' principle is the most appropriate choice.

The calculation can be described by the following relationship:

$$MSD_i = \frac{\sum_{j=1}^{n} \frac{1^n}{y_{ij}^2}}{n} \quad (1)$$

Where: *MSDi* is the mean squared deviation for experiment *i*, y_{ij} is the measured value for setting type *i*, and *n* is the number of replicate (Minitab, 2024).

Based on formula (1), the noise in the experiment was filtered so that, as expected, the higher values are the better (higher tensile stress). The results obtained are given in **Table 3.**

Level	Layer height [mm]	Printing speed [mm/s]	Infill angle [°]
1	744.4	674.8	619.1
2	580.9	657.8	704.7
3	621.1	613.9	622.7
Delta	163.6	60.9	85.6
Rank	1	3	2

Table 3. Average values by calculation

Based on the calculation of average values, a diagram can already be created considering the three variable parameters, from which the main effects can be easily interpreted.

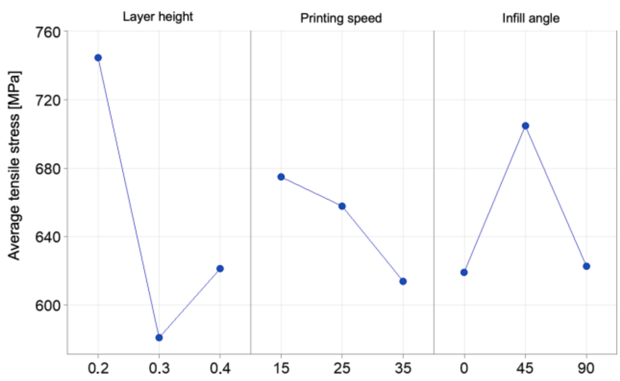

Figure 8. Main effect diagram

From the main effect diagrams **Figure 8**, it is clear that the process parameters with the largest effect are layer height and infill orientation.

To illustrate the cross-effects of the two main influencing factors, an analysis of variance (ANOVA) was performed, where the result of a second-order regression equation on a surface **Figure 9.** Coded units were used to solve the regression equations to compare the interaction of technological parameters of different magnitudes. An analytical method was used to code them into units between -1 and +1 using Minitab software.

If the response surface contains a curvature, a higher degree polynomial model is used.

The second-order regression equation (2):

$$Y=\beta_0+\sum_{i=1}^{k}\beta_i x_i+\sum_{i=1}^{k}\beta_{ii}{x_i}^2+\sum\sum_{i<j}\beta_{ij}x_i x_j+\varepsilon \qquad (2)$$

Where:

- Y - the response variable,
- β_0 - the constant and β_1, β_2, ..., β_k are the coefficients,
- x_1, x_2, ..., x_k - the values of the terms,
- ε - the error term (Minitab, 2024).

Figure 9 illustrates the response surface obtained from the second-order regression analysis, showing the combined effect of the two most influential process parameters—layer height and infill angle—on the tensile strength of the sintered specimens. The curved surface indicates a clear interaction between these parameters. The tensile strength increases with decreasing layer height and moderate infill angles, suggesting that thinner layers improve interlayer bonding while extreme infill orientations may reduce structural integrity. The response surface therefore confirms the findings of the main-effect diagram **Figure 8**, emphasizing that layer height has the dominant influence, while infill angle plays a secondary yet significant role through its interaction with the layer structure.

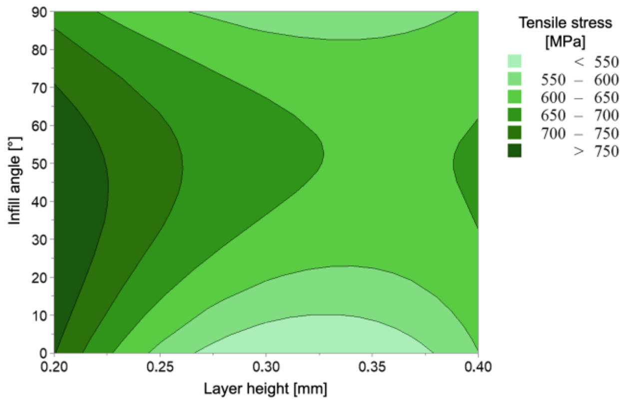

Figure 9. The result of a second-order regression equation on a surface

According to the one-way ANOVA, layer height had a statistically significant effect on tensile strength ($p = 0.033$), indicating that this parameter strongly influences the mechanical performance of sintered parts. Printing speed ($p = 0.748$) and infill angle ($p = 0.481$) did not show statistically significant effects within the examined range.
The macroscopic images show the fracture surfaces of the specimens tested under tension. It can be clearly observed that the fracture surface changes from a finer to a rougher texture as the layer height increases. In addition, for samples printed with larger layer heights, individual filament strands can be seen along the outer surface after fracture, indicating insufficient bonding between the layers. In the following **Figure 10**., from left to right, the specimens with layer heights of 0.2, 0.3, and 0.4 mm are shown.

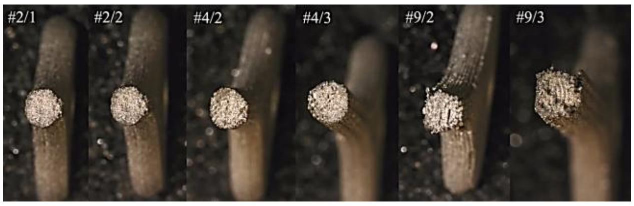

Figure 10. Fracture surfaces of tensile specimens with layer heights of 0.2, 0.3, and 0.4 mm (left to right), showing rougher texture and weaker interlayer bonding with increasing layer height.

During the preparation of the scanning electron microscopy (SEM) images, the primary objective was to capture a relatively larger surface area using the secondary electron (SE) detector in the first step. The microstructural observations were performed on three representative specimens: sample #2 printed with a 0.2 mm layer height, sample #4 with a 0.3 mm layer height, and sample #9 with a 0.4 mm layer height.

At a magnification of 150×, the individual printed layers became clearly distinguishable, allowing detailed observation of the interlayer bonding morphology. In several regions, discontinuities were observed between adjacent layers, indicating imperfect fusion and possible lack of material continuity.

High-magnification (500×) images acquired with the backscattered electron (BSD) detector revealed the presence of fine microscopic porosity and several “foreign” particles embedded within the matrix. These features most likely correspond to residual binder segregation or incomplete removal of the polymeric phase during the debinding process, which may locally influence the mechanical integrity of the sintered parts.

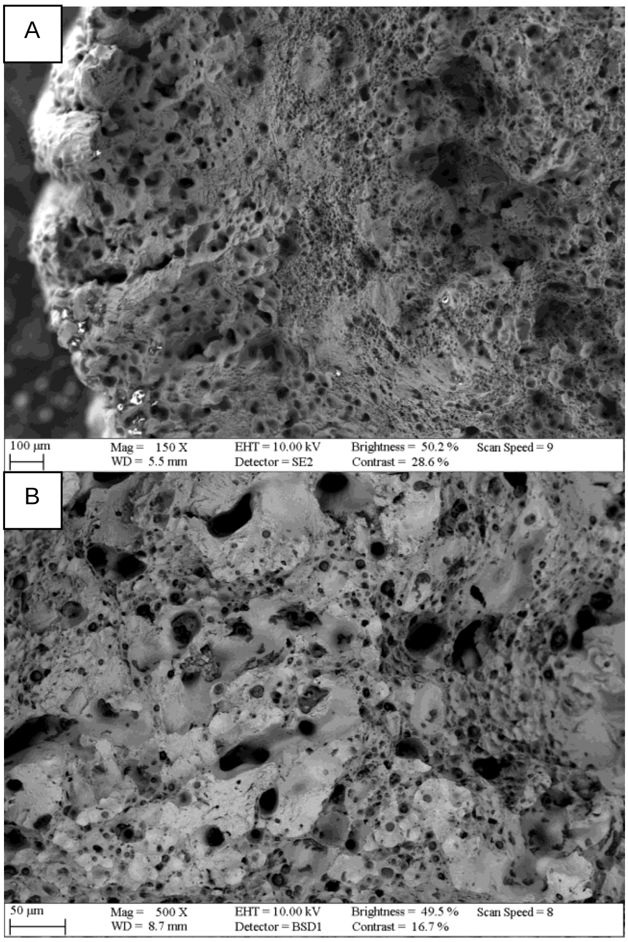

Figure 11 SEM images of sample #2 printed with 0.2 mm layer height; (A) layered structure of the specimen, (B) detailed view of the microstructure.

At lower magnification, the characteristic layered structure of FFF-produced parts can be observed. The boundaries between successive deposited layers are still distinguishable but appear tightly bonded, suggesting proper interlayer fusion during printing and sintering. Some small voids are visible between the layers, most likely caused by incomplete material consolidation or local gas entrapment on **Figure 11/A.** At higher magnification **Figure 11/B**, the microstructure appears fine and uniform, with small spherical and irregular-shaped pores evenly distributed throughout the cross-section. These micro voids most likely originate from binder removal and subsequent sintering shrinkage. Several brighter contrast areas indicate regions of residual binder or local compositional variations. Overall, the 0.2 mm layer height resulted in a finer microstructure with smaller pore size and better material continuity compared to the thicker-layer specimens.

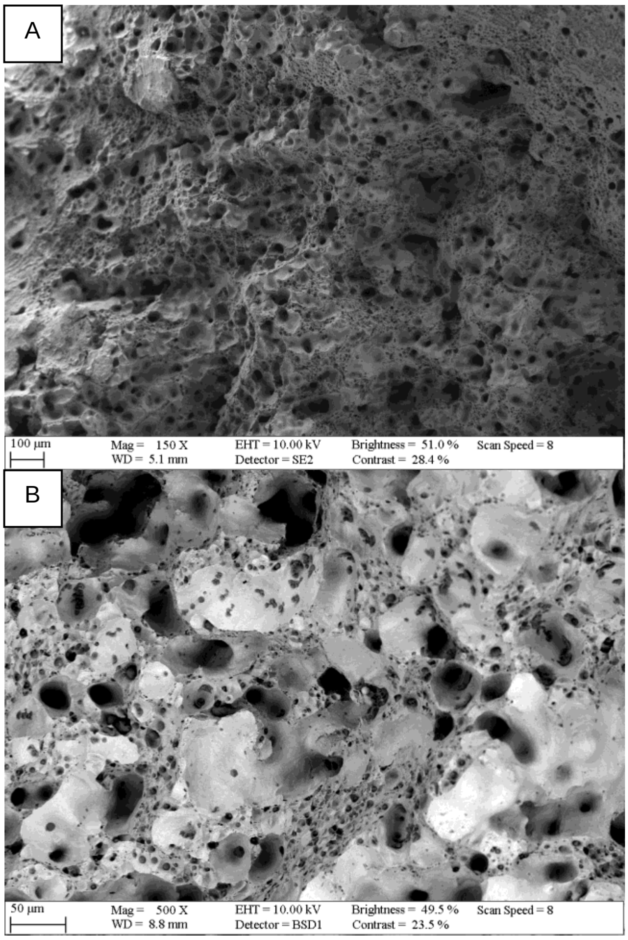

Figure 12. SEM images of sample #4 printed with 0.3 mm layer height; (A) layered structure of the specimen, (B) detailed view of the microstructure.

The layered structure remains visible, but the interfaces between adjacent layers appear less compact than in the thinner-layer sample. Several elongated voids are present along the layer boundaries, indicating a slight deterioration of interlayer fusion as the layer height increases at **Figure 12/A.**
Figure 12/B with higher magnification, the pores appear larger and more irregular compared to the 0.2 mm sample. The pore distribution becomes more heterogeneous, and in some areas the porosity seems interconnected. These features suggest that the increased layer thickness promotes incomplete consolidation and higher local shrinkage during sintering, which can contribute to reduced density and mechanical strength.

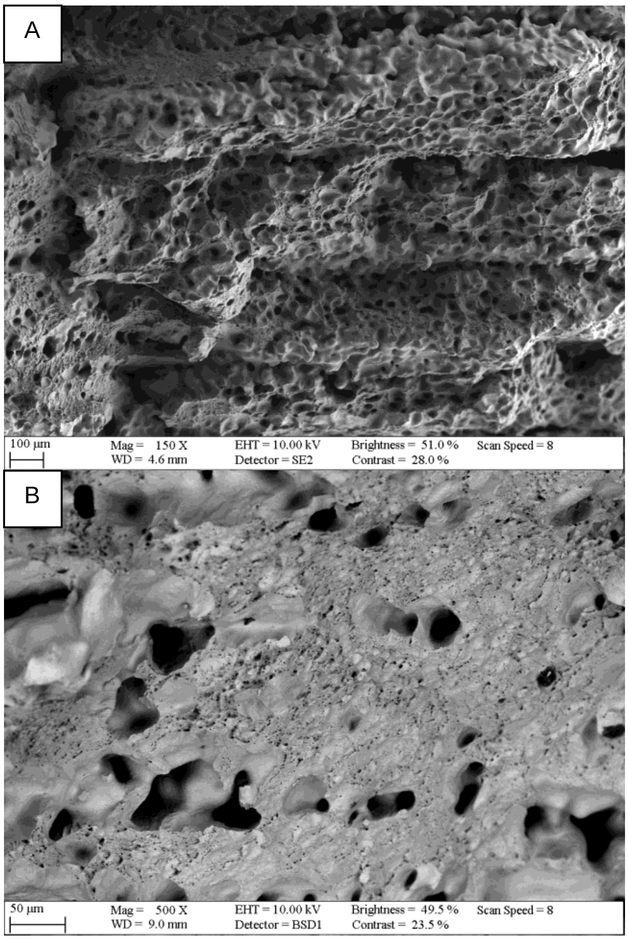

Figure 13. SEM images of sample #9 printed with 0.4 mm layer height; (A) layered structure of the specimen, (B) detailed view of the microstructure.

In the case of the 0.4 mm layer height specimen **Figure 13A and B**, the microstructure shows significantly larger and more irregular pores compared to the thinner-layer samples. The layered morphology is clearly visible, with distinct gaps and discontinuities between the deposited tracks, indicating a weaker interlayer bonding. The pore distribution is highly heterogeneous, and several interconnected voids can be observed, suggesting incomplete densification during sintering. These large voids and irregular features are likely the result of insufficient material fusion and local binder accumulation, leading to reduced mechanical integrity and lower overall strength of the part.

4 CONCLUSION

The experiments demonstrated that among the examined FFF parameters, layer height had the strongest effect on the mechanical properties of sintered 17-4PH stainless steel specimens. The highest tensile strength of 797 MPa was measured at 0.2 mm layer height and 45° infill orientation, while increasing the layer height resulted in a gradual decrease of strength.

The ANOVA analysis confirmed the dominant role of layer height ($p = 0.033$), whereas printing speed and infill angle showed no statistically significant influence. Macroscopic and SEM observations revealed that the fracture surface became noticeably rougher with increasing layer height and unbonded filaments appeared on the outer surface of the thicker layers, indicating weaker interlayer adhesion. These findings are consistent with the mechanical test results and confirm that interlayer bonding quality strongly determines tensile performance.

It should also be noted that the tensile strength values reported in commercial datasheets are typically measured on printed and subsequently machined specimens, which generally exhibit higher mechanical performance. The present study highlights that, in the as-printed condition, the quality of interlayer adhesion plays a decisive role in achieving the expected strength levels. A parameter interaction diagram was developed to illustrate the correlation between process settings and resulting tensile strength, supporting the optimization of FFF-based metal printing.

Future work should include quantitative porosity and density evaluation based on SEM or CT analysis and investigate the origin of interlayer separation observed at higher layer heights.

5 ACKNOWLEDGEMENTS

The experiments were supported by a piece of printer equipment from Craftunique Ltd.

REFERENCES

[Alami 2023] Alami, A.H., et al. Additive manufacturing in the aerospace and automotive industries: Recent trends and role in achieving sustainable development goals. Ain Shams Engineering Journal, 2023, Vol.14, No.11, 102516. https://doi.org/10.1016/j.asej.2023.102516

[Atatreh 2023] Atatreh, S., et al. Evaluation of the infill design on the tensile properties of metal parts produced by fused filament fabrication. Results in Engineering, 2023, Vol.17, 100954. https://doi.org/10.1016/j.rineng.2023.100954

[BASF 2024] BASF. Forward 17-4PH Ultrafuse TDS. 2024. https://forward-am.com/wp-content/uploads/2021/02/Ultrafuse_17-4PH_TDS_EN_v1.1.pdf

[Cho 2023] Cho, Y.-H., et al. 17-4PH stainless steel with excellent strength–elongation combination developed via material extrusion additive manufacturing. Journal of Materials Research and Technology, 2023, Vol.24, pp 3284–3299. https://doi.org/10.1016/j.jmrt.2023.03.228

[Elnik 2024] Elnik System. 2024. https://elnik.com/products/

[Fazzini 2023] Fazzini, F., et al. Correlation between Metal Fused Filament Fabrication parameters and material properties of sintered 17-4 PH. Procedia Structural Integrity, 2023, Vol.49, pp 59–66. https://doi.org/10.1016/j.prostr.2023.10.010

[Forward-AM 2024] Forward-AM. 2024. https://forward-am.com/wp-content/uploads/2021/02/Ultrafuse_17-4PH_TDS_EN_v1.1.pdf

[Galantucci 2022] Galantucci, L.M., et al. 3D Printing of parts using metal extrusion: an overview of shaping debinding and sintering technology. Advanced Technologies & Materials, 2022, Vol.47, No.1, pp 25–32. https://doi.org/10.24867/ATM-2022-1-005

[Henry 2021] Henry, T.C., et al. Mechanical behavior of 17-4 PH stainless steel processed by atomic diffusion additive manufacturing. The International Journal of Advanced Manufacturing Technology, 2021, Vol.114, No.7–8, pp 2103–2114. https://doi.org/10.1007/s00170-021-06785-1

[Kedziora 2022] Kedziora, S., et al. Strength Properties of 316L and 17-4 PH Stainless Steel Produced with Additive Manufacturing. Materials, 2022, Vol.15, No.18, 6278. https://doi.org/10.3390/ma15186278

[Lenth 2001] Lenth, R.V. Introduction to Design and Analysis of Experiments. In The American Statistician, 2001, Vol.55. https://doi.org/10.1198/000313001300339978

[Minitab 2024] Minitab. 2024. https://support.minitab.com/en-us/minitab/21/help-and-how-to/statistical-modeling/doe/how-to/taguchi/analyze-taguchi-design/methods-and-formulas/methods-and-formulas/

[MPIF Standard 2000] MPIF Standard. 2000 In MPIF Standard 50 2000 Materials Standards for Metal Injected Molded Parts.

[Nurhudan 2021] Nurhudan, A.I., et al. Additive manufacturing of metallic based on extrusion process: A review. Journal of Manufacturing Processes, 2021, Vol.66, pp 228–237. https://doi.org/10.1016/j.jmapro.2021.04.018

[Ozsoy 2021] Ozsoy, A., et al. Microstructure and mechanical properties of hybrid additive manufactured dissimilar 17-4 PH and 316L stainless steels. Materials Today Communications, 2021, Vol.28, 102561. https://doi.org/10.1016/j.mtcomm.2021.102561

[Pellegrini 2023] Pellegrini, A., et al. Influence of aging treatments on 17–4 PH stainless steel parts realized using material extrusion additive manufacturing technologies. The International Journal of Advanced Manufacturing Technology, 2023, Vol.126, No.1–2, pp 163–178. https://doi.org/10.1007/s00170-023-11136-3

[Singh 2021a] Singh, G., et al. Additive manufacturing of 17–4 PH steel using metal injection molding feedstock: Analysis of 3D extrusion printing, debinding and sintering. Additive Manufacturing, 2021, Vol.47, 102287. https://doi.org/10.1016/j.addma.2021.102287

[Singh 2021b] Singh, P., et al. Factors affecting properties of Ti-6Al-4V alloy additive manufactured by metal fused filament fabrication. Powder Technology, 2021, Vol.386, pp 9–19. https://doi.org/10.1016/j.powtec.2021.03.026

[Suwanpreecha 2022] Suwanpreecha, C., & Manonukul, A. A Review on Material Extrusion Additive Manufacturing of Metal and How It Compares with Metal Injection Moulding. Metals, 2022, Vol.12, No.3, 429. https://doi.org/10.3390/met12030429

[Xometry 2024] Xometry. 2024. https://www.xometry.com/resources/materials/precipitation-hardening-stainless-steel/

[Zhang 2022] Zhang, Y., & Roch, A. Fused filament fabrication and sintering of 17-4PH stainless steel. Manufacturing Letters, 2022, Vol.33, pp 29–32. https://doi.org/10.1016/j.mfglet.2022.06.004

CONTACTS:

Gyorgy Ledniczky
John von Neumann University
H6000 Kecskemet, Izsaki street 10.
+3676516300, gyorgy.ledniczky@nje.hu
https://nje.hu/en